Picometer-scale atomic shifts governing sub-disordered structures in diamond

Junfeng Cui[1,2], Yingying Yang[3], Mingyang Yang[1], Guoyong Yang[1], Guoxin Chen[2]*, Lei Zhang[2], Cheng-Te Lin[1], Sha Liu[4], Chun Tang[5], Peiling Ke[1,2]*, Yang Lu[6], Kazuhito Nishimura[1], Nan Jiang[1]*

[1] Key Laboratory of Advanced Marine Materials, Ningbo Institute of Materials Technology and Engineering, Chinese Academy of Sciences, Ningbo 315201, China

[2] Public Technology Center, Ningbo Institute of Materials Technology and Engineering, Chinese Academy of Sciences, Ningbo 315201, China

[3] School of Physics and Optoelectronic Engineering, Shandong University of Technology, Zibo 255000, China

[4] State Key Lab of Metastable Materials Science & Technology, College of Materials Science & Engineering, Hebei key lab for optimizing metal product technology and performance, Yanshan University, Qinhuangdao 066004, China

[5] Faculty of Civil Engineering and Mechanics, Jiangsu University, Zhenjiang 212013, China

[6] Department of Mechanical Engineering, The University of Hong Kong, Pokfulam, Hong Kong, China

* Corresponding author. Email: gxchen@nimte.ac.cn (G. X. C.); kepl@nimte.ac.cn (P. L. K.); jiangnan@nimte.ac.cn (N. J.)

Abstract: Diamond is considered as the most promising next-generation semiconductor material due to its excellent physical characteristics. It has been more than three decades since the discovery of a special structure named n-diamond. However, despite extensive efforts, its crystallographic structure and properties are still unclear yet. Here, we show that sub-disordered structures in diamond provide an explanation for the structural feature of n-diamond. Monocrystalline diamond with sub-disordered structures is synthesized via the chemical vapor deposition method. Atomic-resolution scanning transmission electron microscopy characterizations combined with the picometer-precision peak finder technology and diffraction simulations reveal that picometer-scale shifts of atoms within cells of diamond govern the sub-disordered structures. First principles calculations indicate that the bandgap of diamond decreases rapidly with the increasing of shifting distance, in accordance with experimental results. These findings clarify the crystallographic structure and electronic properties of n-diamond, and provide new insights into the bandgap adjustment in diamond.

Keywords: diamond, atomic shift, sub-disordered nanostructure, bandgap, electronic property

Diamond is the hardest natural material, and has great potential applications in high-frequency and high-power electronic devices due to its ultrawide bandgap, high carrier mobility and excellent thermal conductivity[1-3]. Diamond is also considered as the most promising material for quantum technologies because of the nitrogen-vacancy centers, which have unique spin and optical properties[3-6]. With the continuous innovation of the diamond preparation technology, a variety of new structures have been observed in diamond, exhibiting extraordinary performances compared to the best-known traditional cubic structure. For instance, the reported paracrystalline diamond[7] synthesized from zero-dimensional fullerene exhibits preeminent oxidation resistance (950 K of the onset oxidation temperature) and highly isotropous Vickers hardness (116 GPa). The nanotwinned structure[8-9] in diamond improves the hardness up to 200 GPa without sacrificing fracture toughness. The hierarchically structured diamond[10] containing non-3C polytypes (such as 2H, 4H, 9R or 15R) composites exceptional toughness. Furthermore, a special diamond structure (named n-diamond) has been observed for over three decades[11], which has attracted much attention due to its special structural features and potential applications. The electron diffraction pattern of this structure matchs well with that of traditional cubic diamond apart from additional forbidden reflections, the most prominent of which are the (002) diffraction[12]. Nevertheless, details about its crystallographic structure remain debatable, and its properties still unclear.

Since the discovery of n-diamond, plenty of synthesized methods for n-diamond have been reported, and over ten crystal models have been proposed to describe its crystallographic structure[12-13]. To the best of our knowledge, the reported n-diamond is mostly in the form of grains with tiny crystalline size, and mixed with other carbon nanostructures. In addition, experimental investigations for the structure of n-diamond are based on the X-ray powder diffraction (XRD) pattern or the selected area electron diffraction (SEAD) pattern, lacking atomic-resolution characterizations and verifications. Theoretical calculations indicate that most of these proposed crystal models describing the n-diamond are dynamical unstabile[12]. As a result, the Glitter model (space group of P42/mmc)[14] and HR-carbon (space group of R32)[15] model are considered as the most promising candidate structures for n-diamond due to their stabilities. Nevertheless, it is argued that their simulated electron diffraction patterns can not match well with that of n-diamond[13]. It is still a challenge to clarify the detailed structure of n-diamond due to the small quantity, tiny crystalline size and low purity of the synthesized n-diamond[16-18]. The uncertainty of the structure in n-diamond results in little understanding on its physical properties, which limits its developments and applications.

In this study, we synthesized the monocrystalline diamond with partial shifted atoms via the chemical vapor deposition (CVD) method. The atomic shift is verified to be periodic and oriented, rather than random, and the shifting distance is disordered. Thus, we named this structure as sub-disordered structure. The XRD pattern shows a strong (002) forbidden diffraction of standard diamond, in accordance with that of n-diamond. Atomic-resolution scanning transmission electron microscopy (STEM) characterizations combined with the picometer-precision peak finder technology and diffraction simulations were employed to clarify these sub-disordered structures. The formation mechanism and electronic properties of these structures were explored in detail.

Characterizations of sub-disordered structures in diamond. Monocrystalline (001)-diamond samples were synthesized via the CVD method. The Raman spectrum and XRD pattern of the

diamond with sub-disordered structures are depicted in Fig. S1a and Fig. 1a, respectively. The peak of the Raman spectrum at 1332 cm^{-1} corresponds to the vibration of two interpenetrating cubic sublattices, which is consistent with that of traditional diamond[19]. The XRD pattern of the diamond (Fig. 1a) shows a strong diffraction peak at $2\theta = 51°$, corresponding to the (002) diffraction of diamond. It is well known that the (002) diffraction in standard diamond should be absent according to forbidden diffraction rules[20]. For comparison, the XRD pattern of the traditional (001)-diamond and the standard powder diffraction pattern of traditional diamond are demonstrated in Fig. 1b and Fig. 1c, respectively. It can be observed that the XRD pattern of the synthesize (001)-diamond in this study is much distinct from that of traditional (001)-diamond, which shows only the (004) diffraction. The strong (002) diffraction implys there are special structures in the synthesized diamond.

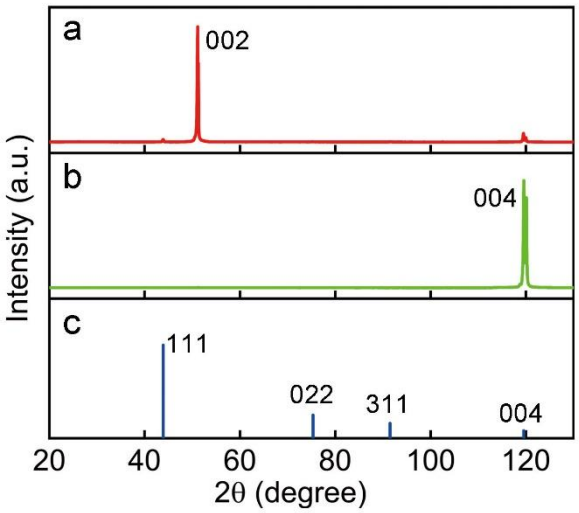

Fig. 1. XRD patterns of diamond with sub-disordered structures and traditional diamond. (**a-b**) Synthesized (001)-diamond with sub-disordered structures (a) and traditional (001)-diamond (b). (**c**) Standard powder diffraction pattern of traditional diamond.

In order to clarify the crystallographic structure of the synthesized diamond, high-resolution STEM characterizations were carried out using an aberration-corrected TEM operating at 300 kV. Fig. 2a demonstrates the SAED pattern of the diamond. The diffraction of {002} agrees well with that in the XRD pattern (Fig. 1a). It's worth noting that, {002} diffraction spots could be observed in the SAED pattern of traditional diamond from {011} or {013} zoon axes due to the double diffraction[20]. Thus, to eliminate the influence of the double diffraction on {002} diffraction spots, the TEM sample is well designed and fabricated from the synthesized monocrystalline (001)-diamond. The diamond zoon axis for TEM characterizations is [100], from which {002} diffraction spots are not attributed to the double diffraction. The diffraction of {420} can also be observed in a brighter image of the SAED pattern (Fig. S2), in accordance with that of n-diamond. Atomic-resolution STEM image of the diamond is depicted in Fig. 2b. In consistent with the SAED pattern in Fig. 2a, the fast Fourier transform (FFT) pattern (the inset in Fig. 2b) shows {002} diffraction spots. It can be seen from the three-dimensional format STEM images (Fig. S3) that there are plenty of fringes with

a spacing of 0.18 nm, corresponding to the interplanar spacing of {002} in diamond[2]. These fringes are in accordance with the FFT pattern and the periodical contrast of atomic columns (Figs. 2b-c), which is attributed to periodical and oriented picometer-scale atomic shifts (discussed in the following section).

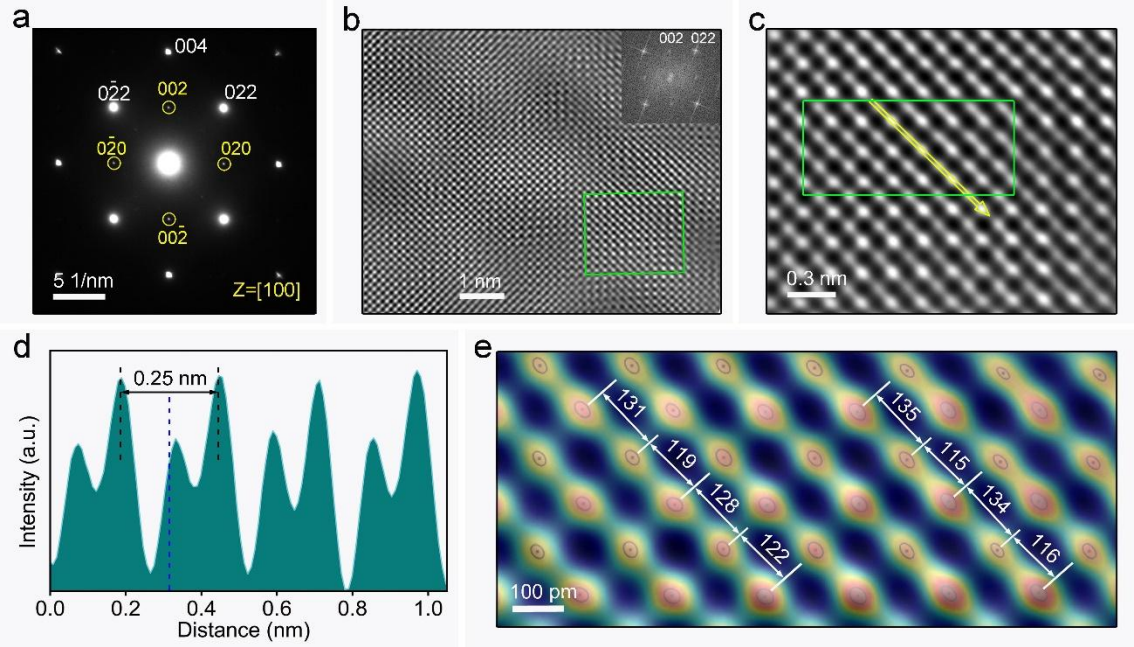

Fig. 2. Atomic-precision characterization on diamond with sub-disordered structures. (**a** and **b**) SAED pattern (a) and atomic-resolution STEM image (b) of the diamond with sub-disordered structures. The inset in (b) shows the corresponding FFT pattern. The {002} diffraction in the SAED pattern and the FFT pattern is in accordance with that of n-diamond. (**c**) Enlarged image taken from the region marked by the green square in (b). (**d**) Intensity line profile of atomic columns marked by the yellow line in (c). The blue dashed line represents the middle position between two black dashed lines. (**e**) Overlap of the atomic-resolution STEM image marked by the green square in (c) and related calculated peak positions of atomic columns employing the multiple-ellipse fitting method.

In order to verify picometer-scale atomic shifts, accurate atomic column positions and intensities in Fig. 2c are analyzed. The intensity line profile of atomic columns along the [01-1] orientation (marked by the yellow line) is shown in Fig. 2d, demonstrating a periodical high-intensity atomic columns with a spacing of 0.25 nm. Obviously, the low-intensity atomic columns deviate from the middle position of two high-intensity atomic columns, where an atomic column should be located at for standard diamond. This suggests that atoms shift along the [01-1] orientation periodically. To quantify the atomic shift, the ultra-high precision peak finder technology was employed, which provided atomic columns positions with picometre-scale precision. This technology has been widely used to measure the atomic displacement at the subunit crystal cell level[21-23]. An overlap of the atomic-resolution STEM image in the region marked by the green square in Fig. 2c and related calculated peak positions of atomic columns is demonstrated in Fig. 2e. Atomic column peak positions (marked by black dots) were calculated by means of the multiple-ellipse fitting method[23].

The multiple-ellipse fitting method is used to help find peak positions of atomic columns in STEM images, for precise measurements of the distance between atomic columns. Assuming the distance between two neighbouring high-intensity atomic columns along the [01-1] orientation is t, the theoretical distance between two neighbouring atomic columns along the [01-1] orientation should be $t/2$. Thus, the shift distance of atomic columns D is calculated as

$$D = |d - t/2| \quad (1)$$

where d is the measured distance between two neighbouring atomic columns along the [01-1] orientation. Based on the measured distances in Fig. 2e and other regions in Fig. S4, the calculated result indicates the atomic columns shift several picometer (3 to 21 pm) along the [01-1] direction. Such slight deviation can be determined thanks to the combination of the ultrahigh-resolution STEM characterization and the ultrahigh-precision peak finder technology. In addition, the STEM image provides the contrast message within the atomic-scale region, in which the contrast arises from atomic columns[20]. As demonstrated in Fig. 2e and Fig. S4, the atomic column intensity is relative fuzzy along the [01-1] direction. This implies atoms deviate along the [01-1] direction, which is verified by the accurate calculation of the distance between peak positions of atomic columns. Thus, it is believed that the atomic shift is oriented. It can be seen from Figs. 2d-e that the deviated and un-deviated atoms are alternatively arranged, suggesting the periodicity of structure in diamond has been changed. This is the reason why the XRD and SAED patterns of the synthesized diamond are distinct from these of traditional diamond.

Atomic shift mechanism. It is well known that the standard diamond lattice can be considered as two interpenetrating face-centered-cubic (FCC) lattices with one displaced by 1/4 of the diagonal along a cubic cell. The unit cell (three-dimensional view) and supper cell (viewed along the [-211] direction) of diamond are depicted in Fig. 3a and Fig. 3b respectively, where the yellow and red balls represent two sets of atoms belonging to the FCC lattice. Using first principles calculations, the lattice constant of diamond was calculated as 3.57 Å, consisting with that in the previous literature[1]. The periodic and oriented structure can be formed when one set of atoms in standard diamond (red balls in Fig. 3a and Fig. 3b) shift along the [01-1] direction by a distance of L, whose unit cell viewed along the [100] direction is shown in Fig. 3c. The driving force will be discussed in the following section. Firstly, the SAED patterns of new structures with different L are simulated to verify that the additional {002} diffraction arises from shifts of atoms. Simulations were performed based on the theory of elastic electron diffraction, and the Bloch-wave method was used to obtain accurate SAED patterns with diffraction intensities[25]. The simulation results are depicted in Fig. 3d. In the case that L=0, the proposed structure is same as standard cubic diamond, thus {002} diffraction spots are absent. When L increases to 2 pm (only 0.4% times $\sqrt{2}a$), the additional {002}

diffraction spots can be observed, which become more and more obvious with the increase of L. To compare with {004} diffraction spots, we define the relative intensity μ of {002} diffraction spots as

$$\mu = \frac{I_{002}}{I_{004}} \tag{2}$$

where I_{002} and I_{004} are simulated intensities of {002} and {004} diffraction spots. Calculated relative intensities of {002} diffraction spots are shown in Fig. 3d.

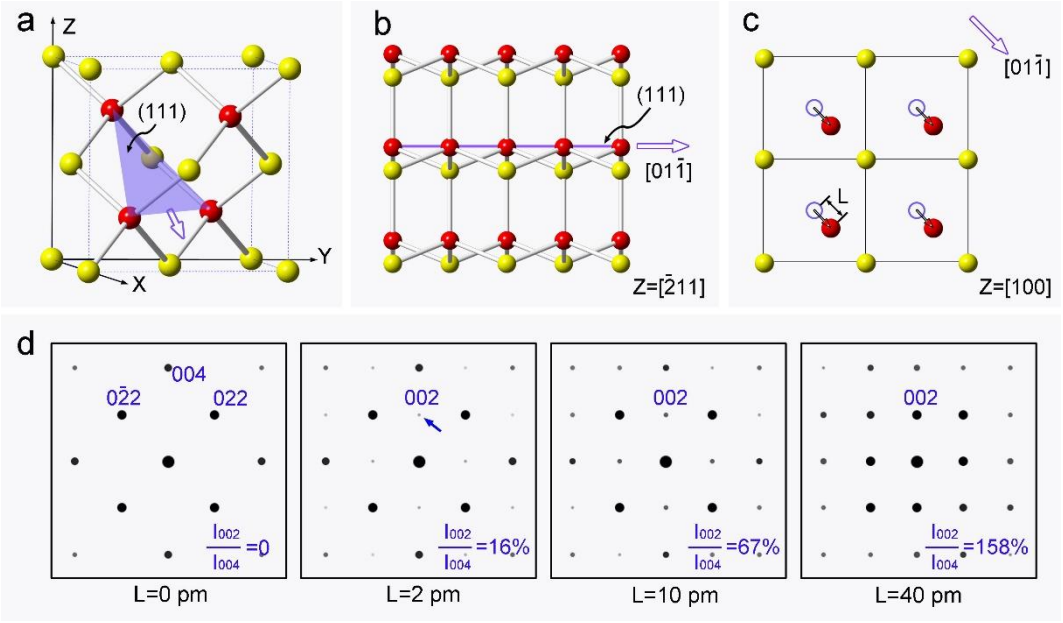

Fig. 3. Simulated SAED patterns of diamond with different atomic shift distance. (**a** and **b**) Unit cell (a) and supercell (b) of standard diamond. The supercell is viewed along the [-211] direction. Two sets of atoms belong to the FCC structure are shown in yellow and red, respectively. (**c**) Unit cell of the structure with atomic shifts in diamond viewed along the [100] direction. Blue circles represent positions of red atoms in standard diamond. (**d**) Simulated SAED patterns of diamond that one set of atoms in unit cell (red atoms in a) shift along the [01-1] direction by a displacement of 0, 2, 10, 40 pm. The simulated zoon axis is [100].

Noting that SAED patterns of structures with different L values are consistent, except for relative intensities of diffraction spots. This implies that additional {002} diffraction spots may arise from a compound of structures with different L, whose intensities depend on the L value and the content of structures with large L values. As a matter of fact, the synthesized diamond contains structures with different L (Fig. 2e and Fig. S4) and the standard diamond structure (Fig. S5). On the other hand, simulated SAED patterns of structures with different L values are consistent can also explain that additional diffraction spots in the experimental SAED pattern are sharp, rather than dispersive. Simulated STEM images of standard diamond and diamond containing structures with different L are shown in Fig. 4. By employing the peak finder technology, centres of atomic columns and distances of adjacent atomic columns in simulated STEM images are calculated. There is no atomic shifting in the standard diamond (Fig. 4a), indicating the high reliability of this technology. Compared with the standard diamond, the atomic column intensity of the simulated STEM image of diamond with

atomic shifting (Fig. 4b) is relative fuzzy along the [01-1] direction. This is consistent with our experimental result in Fig. 2e.

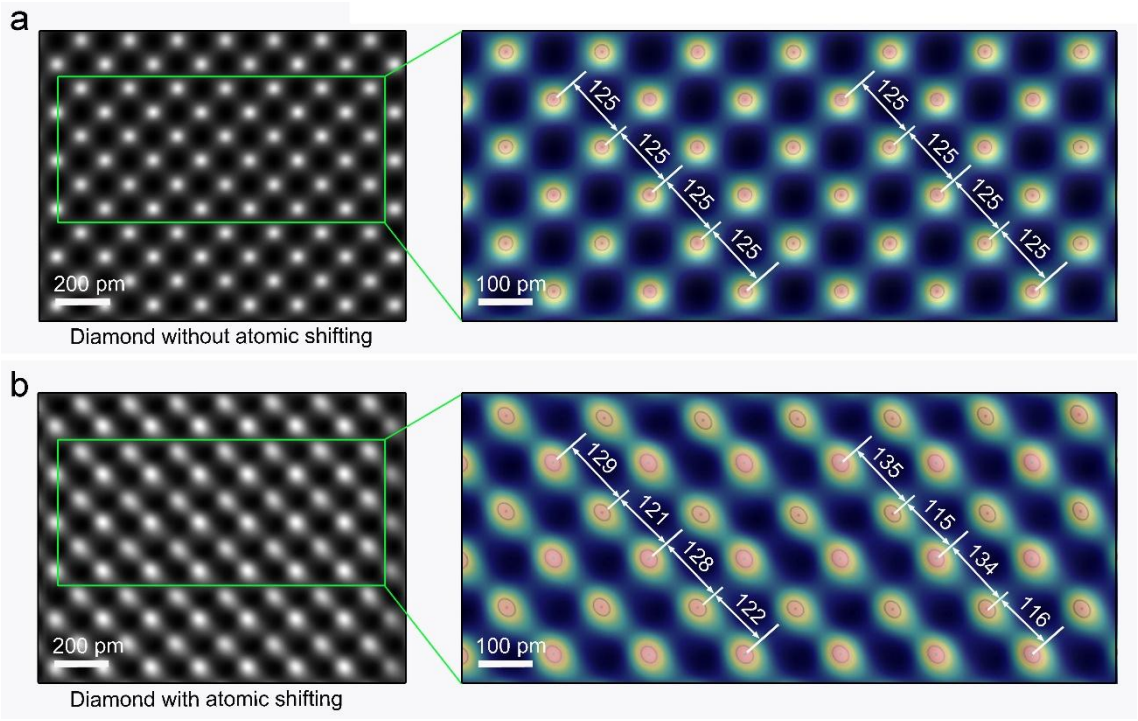

Fig. 4. Simulated STEM images of diamond with and without atomic shifting. (**a**) Simulated STEM image of standard diamond. The right part shows the overlaps of the enlarged STEM image marked by the green square and related calculated peak positions of atomic columns by employing the multiple-ellipse fitting method. (**b**) Simulated STEM image of diamond with atomic shifting. The right part shows the overlaps of the enlarged STEM image marked by the green square and related calculated peak positions of atomic columns by employing the multiple-ellipse fitting method.

Atomic shifts result in slipping in diamond (Supporting Information), and the driving force for the atomic shifts in the synthesized diamond is considered to be the inner stress induced by impurities (such as hydrogen and nitrogen atoms) in the growth process of diamond. It is well known that crystal defects including twins and stacking faults on (111) planes are abundant in CVD diamond[26]. The diamond growths layer by layer, and hydrogen atoms decomposed from H_2 gas would etch non-diamond phases during the growth, ensuring the high purity of the diamond phase. The presence of hydrogen atoms is inevitable to some extent in the CVD diamond. The hydrogen-terminated carbon forms the step edges on (111) planes, which can serve as nucleuses of twins or stacking faults[27]. In this study, nitrogen atoms are introduced in the synthesized diamond with sub-disordered structures. Single substitutional nitrogen defects are verified by the Fourier transform infrared spectra (Fig. S7), and the nitrogen concentration is about 264 ppm. The carbon atoms adjacent to nitrogen and hydrogen suffer from different stress (repulsion and attraction), which will be released by atomic shifts. It also should be noted that the inner stress induced by other impurities (such as the catalyst) or the external stress (such as the shocking compression) during the fabrication of diamond may also

lead to atomic shifts proposed in this study, which are responsible for the additional diffraction of the n-diamond[13]. Noting it has been proposed that the n-diamond is likely to be an H-doped diamond[28], but related structure is still unclear. In this manuscript, we clarify the origin of the n-diamond from the structure point of view.

The above results indicate the periodic and oriented atomic shift associated with n-diamond can be considered as one set of atoms in standard diamond (red balls in Fig. 3a) shift along the [01-1] direction, i.e. atoms on (111) planes shift along the [01-1] direction. In this model, the atom position (Fig. 3c) is consistent with our observations (Figs. 2d-e), and simulated SAED patterns (Fig. 3d) is in accordance with the experimental result (Fig. 2a). What's more, atoms on (111) planes shifting along the [01-1] direction is reasonable, because atoms on the (111) close-packed plane of diamond preferentially slip along the [01-1] close-packed direction. In addition, the effect of atomic shifts on electronic properties of diamond agrees well with experimental results, which will be discussed in the following section.

Effect of atomic shifts on electronic properties of diamond. As mentioned above, picometer-scale atomic shifts are responsible for the additional diffraction of the n-diamond, and atomic shifts are periodic and oriented, which can be considered as one set of atoms in the unit cell of diamond shift along the [01-1] direction. We also studied the effect of atomic shifts on electronic properties of diamond by means of first principles calculations based on density functional theory (DFT). The calculated band structures (Figs. 5a-b) reveal that the bandgap decreases rapidly with the increasing of shifting distance. In particular, the bandgap of standard diamond (L=0 pm) is calculated as 5.5 eV, in accordance with the measurement result based on the Tauc plot method (as mentioned bellow in Fig. S10a). In the diamond structure, a shift of atoms with 10.5 pm results in a decrease in bandgap from 5.5 eV to 3.2 eV, and the bandgap drops to 0.5 eV when atoms shift 17.5 pm. The band structure of diamond is known to be very difficult to be modulated[29]. Because of diamond's low compatibility with other elements, adjusting the bandgap via element doping (especial the n-type doping) is still a challenge for diamond, which has been maturely used in other semiconductor materials such as silicon[30] and silicon carbide[31]. Strain engineering is another strategy for the bandgap adjustment in semiconductor materials. Nevertheless, large strain is not easy to be achieved in diamond due to its hard and brittle characteristics. Diamond's bandgap dropped to 3.1 eV from 5.3 eV at 9% tensile strain, which is the reported largest bandgap reduction rate[1]. Thus, the rapid decrease in bandgap (Fig. 5b) induced by picometer-scale atomic shifts opens up a new route to modulate diamond's electronic properties, and provide a new insight into the bandgap adjustment in diamond.

To gain further insights into electronic properties of diamond with atomic shifts, we performed the density of states (DOS) calculations. It can be observed from the DOS plots of selected structures (Fig. 5c) that the onset position of band states (as indicated by the green arrow) after the valence

band maximum moves left with the increase of the shifting distance, indicating the conduction band minimum drops, which leads to the decrease in bandgap. This is in accordance with the calculated band structures in Fig. 5a. A further increase of the shifting distance results in a large amount of band states near the valence band maximum, implying the high electrical conductivity of diamond[32]. In Fig. 5d, we show valence charge density distributions of diamond with different shifting distances. Picometer-scale atomic shifts lead to the charge redistribution, which is responsible for the decrease in bandgap and enhancement in electrical conductivity of diamond.

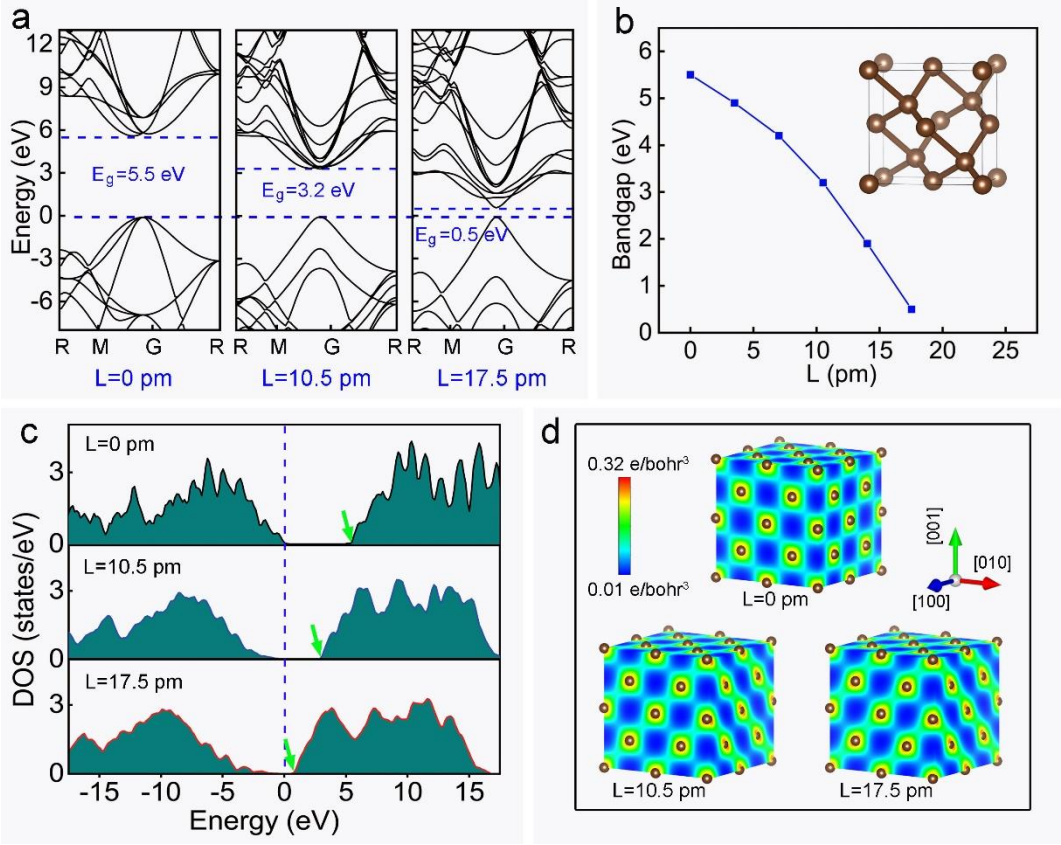

Fig. 5. DFT calculated electronic features of structures in diamond with atomic shifting. (**a**) Band structures of diamond that one set of atoms in unit cell (red atoms in Fig. 3c) shift along the [01-1] direction by a distance of 0, 10.5 and 17.5 pm. (**b**) Calculated bandgap as a function of shift distance in diamond. The inset shows an unit cell of diamond with atomic shifting. (**c**) DOS plots of diamond that one set of atoms in unit cell shift along the [01-1] direction by a distance of 0, 10.5 and 17.5 pm. The vertical dashed line represents the valence band maximum. (**d**) Valence charge density distributions of the traditional diamond (L=0 pm) and the diamond with atomic shifting (L=10.5 pm, L=17.5 pm).

Atomic shifts dominating the bandgap decrease and electrical conductivity enhancement are verified by high-resolution STEM electron energy-loss spectroscopy (EELS) characterizations, Tauc plots and current-voltage measurements. Low-energy EELS spectra (Fig. S8) were taken from three different spots in the synthesized diamond with sub-disordered structures, and the bandgap was directly determined from the spectra. The bandgap at spot 1 was measured as 3.6 eV, much lower

than that at spot 2 (4.8 eV) and spot 3 (5.5 eV). As mentioned above, the diamond contains structures with different shifting distances (Fig. 2e) and the standard diamond structure (Fig. S5), and DFT calculations indicate a small diversity in shifting distance can lead to a large difference in bandgap (Fig. 5). The STEM-EELS spectra are taken from regions at the atomic scale, and the atomic shift distance is various, which is responsible for the variation in bandgap. Thus, the decreased bandgap and its variation are in in accordance with the above DFT results.

The decrease in bandgap of the diamond with atomic shifts is further verified by the Tauc plot method, which has been considered as one of the most common methods to determine the bandgap of semiconductors[33-34]. As one can seen from the Tauc plots in Fig. S9, the measured bandgap of the diamond with atomic shifts is 2.3 eV, much lower than that of the traditional diamond (5.5 eV). In addition, it can be seen from the measured current-voltage curves (Fig. S10) that the diamond with atomic shifts is much conductive compared with the standard diamond. The tested conductivity of the diamond with atomic shifts (7.7×10^{14} Ω·cm) is about 10^6 times greater that that of the traditional diamond (7.3×10^8 Ω·cm). Noting that the measured bandgap (using the Tauc plot method) and the current-voltage curve of the diamond with atomic shifts show the electrical property at the macro-scale, and the diamond specimen contains structures with different shifting distances. In other words, the measured electrical property of macro-specimen is a mixture of the properties of structures with different shifting distances, and the results are consistent with our DFT results that the atomic shift leads to the decrease in bandgap and the increase in the conductivity of diamond. On the other hand, we attribute the atomic shifting in diamond to the inner stress induced by impurities, and the atomic shifts of the pure carbon lead to the decrease in bandgap (DFT results) explains the intrinsic reason why impurities would change the electronic structure and bandgap of diamond from the structure point of view.

In conclusion, the monocrystalline diamond with sub-disordered structures was synthesized via the CVD method. The diamond shows an additional strong (002) diffraction in the XRD pattern, associated with n-diamond. This is attributed to picometer-scale atomic shifts within cells of diamond, and the atomic shift is verified to be periodic and oriented, rather than random, and the shifting distance is disordered. Diffraction simulations demonstrate that intensities of {002} diffractions increase with the increasing of shifting distance. DFT calculations reveal that the glide with anti-shuffle of (111) planes along the [01-1] direction dominates the atomic shifts in diamond. Additionally, effects of the atomic shift on electronic properties of diamond are also uncovered. First principles calculations indicate the diamond's bandgap decreases rapidly with the increasing of shifting distance, which drops to 0.5 eV when atoms shift 17.5 pm. The picometer-scale atomic shifts lead to the charge redistribution, resulting in the change of electronic properties. Atomic shifts dominating the bandgap decrease and electrical conductivity enhancement are verified by high-resolution STEM electron energy-loss spectroscopy characterizations, Tauc plots and current-voltage measurements. These structures with atomic shifts may have other extraordinary features and

properties, which need a further deep investigation. These results provide a structure basics for further investigations, and are valuable to modulate diamond's electronic properties and develop high-performance diamond and related devices.

ASSOCIATEDCONTENT

Supporting Information

The Supporting Information is available free of charge at xxxxxx.

Materials and methods, including diamond fabrication, characterizations (XRD patterns, Raman and photoluminescence spectra, Fourier transform infrared and ultraviolet-visible transmission spectrum as well as current-voltage measurements, TEM characterizations), and DFT calculations; Slipping behavior and related mechanism in diamond.

ASSOCIATEDCONTENT

Corresponding Authors

Guoxin Chen - Public Technology Center, Ningbo Institute of Materials Technology and Engineering, Chinese Academy of Sciences, Ningbo 315201, China

Email: gxchen@nimte.ac.cn

Peiling Ke - Key Laboratory of Advanced Marine Materials, Ningbo Institute of Materials Technology and Engineering, Chinese Academy of Sciences, Ningbo 315201, China; Public Technology Center, Ningbo Institute of Materials Technology and Engineering, Chinese Academy of Sciences, Ningbo 315201, China

Email: kepl@nimte.ac.cn

Nan Jiang - Key Laboratory of Advanced Marine Materials, Ningbo Institute of Materials Technology and Engineering, Chinese Academy of Sciences, Ningbo 315201, China

Email: jiangnan@nimte.ac.cn

Authors

Junfeng Cui - Key Laboratory of Advanced Marine Materials, Ningbo Institute of Materials Technology and Engineering, Chinese Academy of Sciences, Ningbo 315201, China; Public Technology Center, Ningbo Institute of Materials Technology and Engineering, Chinese Academy of Sciences, Ningbo 315201, China; orcid.org/0000-0002-3564-6288

Yingying Yang - School of Physics and Optoelectronic Engineering, Shandong University of Technology, Zibo 255000, China

Mingyang Yang - Key Laboratory of Advanced Marine Materials, Ningbo Institute of Materials Technology and Engineering, Chinese Academy of Sciences, Ningbo 315201, China

Guoyong Yang - Key Laboratory of Advanced Marine Materials, Ningbo Institute of Materials Technology and Engineering, Chinese Academy of Sciences, Ningbo 315201, China

Lei Zhang - Public Technology Center, Ningbo Institute of Materials Technology and Engineering, Chinese Academy of Sciences, Ningbo 315201, China

Cheng-Te Lin - Key Laboratory of Advanced Marine Materials, Ningbo Institute of Materials Technology and Engineering, Chinese Academy of Sciences, Ningbo 315201, China; orcid.org/ orcid.org/0000-0002-7090-9610
Sha Liu - State Key Lab of Metastable Materials Science & Technology, College of Materials Science & Engineering, Hebei key lab for optimizing metal product technology and performance, Yanshan University, Qinhuangdao 066004, China
Chun Tang - Faculty of Civil Engineering and Mechanics, Jiangsu University, Zhenjiang 212013, China; orcid.org/ orcid.org/0000-0002-7767-2126
Yang Lu - Department of Mechanical Engineering, The University of Hong Kong, Pokfulam, Hong Kong, China; orcid.org/ orcid.org/0000-0002-9280-2718
Kazuhito Nishimura - Key Laboratory of Advanced Marine Materials, Ningbo Institute of Materials Technology and Engineering, Chinese Academy of Sciences, Ningbo 315201, China

ACKNOWLEDGMENTS

The authors acknowledge the financial supports from the National Natural Science Foundation of China (52302203), the Zhejiang Province Natural Science Foundation of China (LQ24E020006), the China Postdoctoral Science Foundation (2022M723248), the Ningbo Natural Science Foundation (2023J336), the National Key R&D Program of China (2022YFB3706602, 2021YFB3701801), the Science and Technology Major Project of Ningbo (2021ZDYF020196, 2021ZDYF020198). Y.Y. Yang acknowledges the support from the Natural Science Foundation of Shandong Province (ZR2022QA062) and the National Natural Science Foundation of China (12304228). S. Liu acknowledges the support from the Hebei Natural Science Foundation (E2023203179) and the Science and Technology Project of Hebei Education Department (BJK2024002). Y. Lu acknowledges the support from the Research Grants Council of the Hong Kong Special Administrative Region, China, under project # RFS2021-1S05.

REFERENCES

1. Dang C.Q., Chou J.P., Dai B., Chou C.T., Yang Y., Fan R., Lin W.T., Meng F.L., Hu A., Zhu J.Q., Han J.C., Minor A.M., Li J., Lu Y. Achieving large uniform tensile elasticity in microfabricated diamond. *Science* 2021, 371 (6524), 76-78.
2. Nie A., Bu Y., Li P., Zhang Y., Jin T., Liu J., Su Z., Wang Y., He J., Liu Z., Wang H., Tian Y., Yang W. Approaching diamond's theoretical elasticity and strength limits. *Nat. Commun.* 2019, 10 (1), 5533.
3. Yang J., Liu K., Chen X., Shen D. Recent advances in optoelectronic and microelectronic devices based on ultrawide-bandgap semiconductors. *Prog. Quant. Electron.* 2022, 83, 100397.
4. Hamlin J.J., Zhou B.B. Extreme diamond-based quantum sensors. *Science* 2019, 366 (6471), 1312-1313.
5. Sherman A., Zgadzai O., Koren B., Peretz I., Laster E., Blank A. Diamond-based microwave quantum amplifier. *Sci. Adv.* 2022, 8 (49), eade6527.
6. Liu K., Zhang S., Ralchenko V., Qiao P., Zhao J., Shu G., Yang L., Han J., Dai B., Zhu J. Tailoring of typical color centers in diamond for photonics. *Adv. Mater.* 2021, 33 (6), e2000891.

7. Tang H., Yuan X., Cheng Y., Fei H., Liu F., Liang T., Zeng Z., Ishii T., Wang M.S., Katsura T., Sheng H., Gou H. Synthesis of paracrystalline diamond. *Nature* 2021, 599 (7886), 605-610.
8. Huang Q., Yu D., Xu B., Hu W., Ma Y., Wang Y., Zhao Z., Wen B., He J., Liu Z., Tian Y. Nanotwinned diamond with unprecedented hardness and stability. *Nature* 2014, 510 (7504), 250-3.
9. Tong K., Zhang X., Li Z., Wang Y., Luo K., Li C., Jin T., Chang Y., Zhao S., Wu Y., Gao Y., Li B., Gao G., Zhao Z., Wang L., Nie A., Yu D., Liu Z., Soldatov A., Hu W., Xu B., Tian Y. Structural transition and migration of incoherent twin boundary in diamond. Nature (2024). https://doi.org/10.1038/s41586-023-06908-6
10. Yue Y., Gao Y., Hu W., Xu B., Wang J., Zhang X., Zhang Q., Wang Y., Ge B., Yang Z., Li Z., Ying P., Liu X., Yu D., Wei B., Wang Z., Zhou X.F., Guo L., Tian Y. Hierarchically structured diamond composite with exceptional toughness. *Nature* 2020, 582 (7812), 370-374.
11. Hirai K., Kondo I. Modified phases of diamond formed under shock compression and rapid quenching. *Science* 1991, 253 (5021), 772-774.
12. Baldissin G., Bull D.J. N-diamond: dynamical stability of proposed structures. *Diam. Relat. Mater.* 2013, 34, 60-64.
13. Wen B., Zhao J.J., Li T.J. Synthesis and crystal structure of n-diamond. *Int. Mater. Rev.* 2007, 52 (3), 131-151.
14. Bucknum M.J., Stamatin I., Castro E.A. A chemically intuitive proposal for the structure of n-diamond. *Mol. Phys.* 2005, 103 (20), 2707-2715.
15. Li D., Tian F., Chu B., Duan D., Sha X., Lv Y., Zhang H., Lu N., Liu B., Cui T. Ab initio structure determination of n-diamond. *Sci. Rep.* 2015, 5, 13447.
16. Dai D., Li Y., Fan J. Room-temperature synthesis of various allotropes of carbon nanostructures (graphene, graphene polyhedra, carbon nanotubes and nano-onions, n-diamond nanocrystals) with aid of ultrasonic shock using ethanol and potassium hydroxide. *Carbon* 2021, 179, 133-141.
17. Xiao J., Li J.L., Liu P., Yang G.W. A new phase transformation path from nanodiamond to new-diamond via an intermediate carbon onion. *Nanoscale* 2014, 6 (24), 15098-106.
18. Kumar A., Lin P.A, Xue A., Hao B.Y., Yap Y.K., Sankaran R.M. Formation of nanodiamonds at near-ambient conditions via microplasma dissociation of ethanol vapour. *Nat. Commun.* 2013, 4, 2618.
19. Prawer S., Nemanich R.J. Raman spectroscopy of diamond and doped diamond. *Phil. Trans. R. Soc. A.* 2004, 362 (1824), 2537-2565.
20. Williams D.B., Carter C.B. Transmission electron microscopy: a textbook for materials science. *Springer* 2009, 978-0-387-76500-6.
21. Sun Y.W., Abid A.Y., Tan C.B., Ren C.L., Li M.Q., Li N., Chen P., Li Y.H., Zhang J.M., Zhong X.L., Wang J.B., Liao M., Liu K.H., Bai X.D., Zhou Y.C., Yu D.P., Gao P., Subunit cell-level measurement of polarization in an individual polar vortex. *Sci. Adv.* 2019, 5, eaav4355.
22. Jiang H., Qi J., Wu D., Lu W., Qian J., Qu H., Zhang Y., Liu P., Liu X., Chen L. Atomic-resolution characterization on the structure of strontium doped barium titanate nanoparticles. *Nano Res.* 2021, 14 (12), 4802-4807.
23. Tang Y. L., Zhu Y.L., Ma X.L., Borisevich A.Y., Morozovska A.N., Eliseev E.A., Wang W.Y., Wang Y.J., Xu Y.B., Zhang Z.D., Pennycook S.J. Observation of a periodic array of flux-closure quadrants in strained ferroelectric $PbTiO_3$ films. *Science* 2015, 348 (6234), 547-551.
24. Zhang Q., Jin C.H., Xu H.T., Zhang L.Y., Ren X.B., Ouyang Y., Wang X.J., Yue X.J., Lin F. Multiple-ellipse fitting method to precisely measure the positions of atomic columns in a transmission electron microscope image. *Micron* 2018, 113, 99-104.

25. Gratias D., Portier R. Time-link perturbation method in high-energy electron-diffraction. *Acta Cystallogr. A* 1983, 39, 576-584.
26. Kaboli S., Burnley P.C. Direct observations of crystal defects in polycrystalline diamond. *Mater. Charact.* 2018, 142, 154-161.
27. Butler J. E., Oleynik I. A mechanism for crystal twinning in the growth of diamond by chemical vapour deposition. *Philos. T. R. Soc. A* 2008, 366 (1863), 295-311.
28. Wen, B., Melnik, R., Yao, S., Li, T.J. Hydrogen-doped cubic diamond and the crystal structure of n-diamond. *Chem. Phys. Lett.* 2011, 516, 230-232.
29. Dang C.Q., Lu, A.L., Wang H.Y., Yang L.M., Li X.C., Zhang H.T., Lu, Y. Extreme mechanics of nanoscale diamond towards functional device applications. *Extreme Mech. Lett.* 2023, 58, 101931.
30. Luo Z., Liu B., Li H., Chang X., Zhu W., Wang T., Gong J. Multifunctional nickel film protected n-type silicon photoanode with high photovoltage for efficient and stable oxygen evolution reaction. *Small Methods* 2019, 3 (10), 1900212.
31. Karadavut O., Chaudhuri S.K., Kleppinger J.W., Nag R., Mandal K.C. Enhancement of radiation detection performance with reduction of EH6/7 deep levels in n-type 4H-SiC through thermal oxidation. *Appl. Phys. Lett.* 2022, 121 (1), 012103.
32. Liu C., Song X., Li Q., Ma Y., Chen C. Superconductivity in compression-shear deformed diamond. *Phys. Rev. Lett.* 2020, 124 (14), 147001.
33. Makula P., Pacia M., Macyk W. How to correctly determine the band gap energy of modified semiconductor photocatalysts based on UV-vis spectra. *J. Phys. Chem. Lett.* 2018, 9, 6814-6817.
34. Ren G.P., Sun M.Y., Sun Y., Li Y., Wang C.Q., Lu A.H., Ding H.R. A cost-effective birnessite-silicon solar cell hybrid system with enhanced performance for dye decolorization. *RSC Adv.* 2017, 7, 47975-47982.

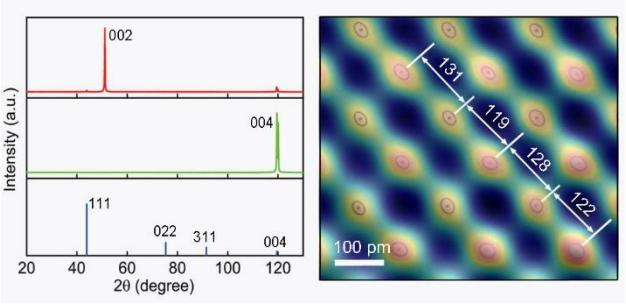

TOC